

# Hidden Physics Models: Machine Learning of Nonlinear Partial Differential Equations

Maziar Raissi and George Em Karniadakis

*Division of Applied Mathematics, Brown University,  
Providence, RI, 02912, USA*

---

## Abstract

We introduce the concept of *hidden physics models*, which are essentially data-efficient learning machines capable of leveraging the underlying laws of physics, expressed by time dependent and nonlinear partial differential equations, to extract patterns from high-dimensional data generated from experiments. The proposed technology is applied to the problem of learning, system identification, or data-driven discovery of partial differential equations. The framework relies on Gaussian processes, a powerful tool for probabilistic inference over functions, to strike a balance between model complexity and data fit. The effectiveness of the proposed approach is demonstrated through a variety of canonical problems, spanning a number of scientific domains, including the Navier-Stokes, Schrödinger, Kuramoto-Sivashinsky, and fractional equations. The methodology provides a promising new direction for capitalizing on the long-standing developments of classical methods in applied mathematics and mathematical physics to design learning machines with the ability to learn in complex domains without requiring large quantities of data.

*Keywords:* probabilistic machine learning, system identification, backward Euler, Bayesian modeling, uncertainty quantification

---

## 1. Introduction

Data-driven methods, which have been enabled in the past decade by the plummeting cost of sensors, data storage, and computational resources, are taking center stage across many disciplines of science. We now have highly scalable solutions for problems in object detection and recognition, machine

translation, text-to-speech, recommender systems, and information retrieval. All of these solutions attain state-of-the-art performance when trained with large amounts of data. However, purely data driven approaches for machine learning present difficulties when the data is scarce relative to the complexity of the system. As an example, consider a robotic spacecraft that does not orbit the Earth, but, instead, explores further into outer space. The ability to learn in a sample-efficient manner is a necessity in these data-limited domains. Less well understood is how to leverage the underlying physical laws and/or governing equations to extract patterns from scarce data generated from highly complex systems. In this work, we propose a modeling framework that enables blending conservation laws, physical principles, and/or phenomenological behaviors expressed by partial differential equations with the data-sets available in many fields of engineering, science and technology. This paper should be considered a direct continuation of a preceding one [1] in which we addressed the problem of inferring solutions of time dependent and nonlinear partial differential equations using noisy observations. Here, a similar technology is employed to deal with the problem of learning, system identification, or data-driven discovery of partial differential equations [2].

## 2. Problem Setup

Let us consider parametrized and nonlinear partial differential equations of the general form

$$h_t + \mathcal{N}_x^\lambda h = 0, \quad x \in \Omega, \quad t \in [0, T], \quad (1)$$

where  $h(t, x)$  denotes the latent (hidden) solution,  $\mathcal{N}_x^\lambda$  is a nonlinear operator parametrized by  $\lambda$ , and  $\Omega$  is a subset of  $\mathbb{R}^D$ . As an example, the one dimensional Burgers' equation corresponds to the case where  $\mathcal{N}_x^\lambda h = \lambda_1 h h_x - \lambda_2 h_{xx}$  and  $\lambda = (\lambda_1, \lambda_2)$ . Here, the subscripts denote partial differentiation in either time or space. Given noisy measurements of the system, one is typically interested in the solution of two distinct problems. The first problem is that of inference or filtering and smoothing, which asks: given fixed model parameters  $\lambda$  what can be said about the unknown hidden state  $h(t, x)$  of the system? This question is the topic of a preceding paper [1] of the authors in which we introduce the concept of *numerical Gaussian processes* and address the problem of inferring solutions of time dependent and nonlinear partial differential equations using noisy observations. The second problem is that

of learning, system identification, or data driven discovery of partial differential equations [2] which asks: what are the parameters  $\lambda$  that best describe the observed data? Here we assume that all we observe are two snapshots  $\{\mathbf{x}^{n-1}, \mathbf{h}^{n-1}\}$  and  $\{\mathbf{x}^n, \mathbf{h}^n\}$  of the system at times  $t^{n-1}$  and  $t^n$ , respectively, that are  $\Delta t = t^n - t^{n-1}$  apart. The main assumption is that  $\Delta t$  is small enough so that we can apply the backward Euler time stepping scheme to equation (1) and write

$$h^n + \Delta t \mathcal{N}_x^\lambda h^n = h^{n-1}. \quad (2)$$

Here,  $h^n(x) = h(t^n, x)$  is the hidden state of the system at time  $t^n$ . Approximating the nonlinear operator on the left hand side of equation (2) by a linear one we obtain

$$\mathcal{L}_x^\lambda h^n = h^{n-1}. \quad (3)$$

For instance, the nonlinear operator

$$h^n + \Delta t \mathcal{N}_x^\lambda h^n = h^n + \Delta t (\lambda_1 h^n h_x^n - \lambda_2 h^n),$$

involved in the Burgers' equation can be approximated by the linear operator

$$\mathcal{L}_x^\lambda h^n = h^n + \Delta t (\lambda_1 h^{n-1} h_x^n - \lambda_2 h^n),$$

where  $h^{n-1}(x)$  is the state of the system at the previous time  $t^{n-1}$ .

### 3. The Basic Model

Similar to Raissi et al. [3, 4], we build upon the fortunate analytical property of Gaussian processes that the output of a linear system whose input is Gaussian distributed is again Gaussian. Specifically, we proceed by placing a Gaussian process [5] prior over the latent function  $h^n(x)$ ; i.e.,

$$h^n(x) \sim \mathcal{GP}(0, k(x, x', \theta)). \quad (4)$$

Here,  $\theta$  denotes the hyper-parameters of the covariance function  $k$ . Gaussian process regression (see [5, 6]) is a non-parametric Bayesian machine learning technique that provides a flexible prior distribution over functions, enjoys analytical tractability, and has a fully probabilistic work-flow that returns robust posterior variance estimates, which quantify uncertainty in a natural way. Moreover, Gaussian processes are among a class of methods known as

kernel machines (see [7, 8, 9]) and are analogous to regularization approaches (see [10, 11, 12]). They can also be viewed as a prior on one-layer feed-forward Bayesian neural networks with an infinite number of hidden units [13]. The Gaussian process prior assumption (4) along with equation (3) enables us to capture the entire structure of the operator  $\mathcal{L}_x^\lambda$  in the resulting multi-output Gaussian process

$$\begin{bmatrix} h^n \\ h^{n-1} \end{bmatrix} \sim \mathcal{GP} \left( 0, \begin{bmatrix} k^{n,n} & k^{n,n-1} \\ k^{n-1,n} & k^{n-1,n-1} \end{bmatrix} \right). \quad (5)$$

It is worth highlighting that the parameters  $\lambda$  of the operators  $\mathcal{L}_x^\lambda$  and  $\mathcal{N}_x^\lambda$  turn into hyper-parameters of the resulting covariance functions. The specific forms of the kernels

$$\begin{aligned} k^{n,n}(x, x'; \theta), & & k^{n,n-1}(x, x'; \theta, \lambda), \\ k^{n-1,n}(x, x'; \theta, \lambda), & & k^{n-1,n-1}(x, x'; \theta, \lambda), \end{aligned}$$

are direct functions of equation (3) as well as the prior assumption (4); i.e.,

$$\begin{aligned} k^{n,n} &= k, & k^{n,n-1} &= \mathcal{L}_{x'}^\lambda k, \\ k^{n-1,n} &= \mathcal{L}_x^\lambda k, & k^{n-1,n-1} &= \mathcal{L}_x^\lambda \mathcal{L}_{x'}^\lambda k, \end{aligned}$$

We call the multi-output Gaussian process (5) a *hidden physics model*, because its matrix of covariance functions explicitly encodes the underlying laws of physics expressed by equations (1) and (3). Moreover, without loss of generality, all Gaussian process priors (see e.g., equation (4)) used in this work are assumed to have a squared exponential covariance function, i.e.,

$$k(x, x'; \theta) = \gamma^2 \exp \left( -\frac{1}{2} \sum_{d=1}^D w_d^2 (x_d - x'_d)^2 \right),$$

where  $\theta = (\gamma, w_1, \dots, w_D)$  are the hyper-parameters and  $x$  is a  $D$ -dimensional vector. From a theoretical point of view, each kernel gives rise to a Reproducing Kernel Hilbert Space [14, 15, 16] that defines a class of functions that can be represented by this kernel. In particular, the squared exponential covariance function chosen above implies smooth approximations. More complex function classes can be accommodated by appropriately choosing kernels. For example, non-stationary kernels employing nonlinear warping of the in-

put space can be constructed to capture discontinuous response [17, 18]. In general, the choice of kernels is crucial and in many cases still remains an art that relies on one’s ability to encode any prior information (such as known symmetries, invariances, etc.) into the regression scheme. In this work, this prior information is the knowledge of the operator  $\mathcal{L}_x^\lambda$  itself. Starting, for example, from a base square exponential kernel and applying  $\mathcal{L}_x^\lambda$  as described above, one obtains a prior that is adapted to the linear operator and inherits its underlying structure. Our empirical findings so far indicate that this procedure is quite robust and insensitive to the choice of the base kernel, although this observation should be interpreted as a conjecture rather than a firm result.

#### 4. Learning

Given the noisy data  $\{\mathbf{x}^{n-1}, \mathbf{h}^{n-1}\}$  and  $\{\mathbf{x}^n, \mathbf{h}^n\}$  on the latent solution at times  $t^{n-1}$  and  $t^n$ , respectively, the hyper-parameters  $\theta$  of the covariance functions and more importantly the parameters  $\lambda$  of the operators  $\mathcal{L}_x^\lambda$  and  $\mathcal{N}_x^\lambda$  can be learned by employing a Quasi-Newton optimizer L-BFGS [19] to minimize the negative log marginal likelihood [5]

$$-\log p(\mathbf{h}|\theta, \lambda, \sigma^2) = \frac{1}{2}\mathbf{h}^T \mathbf{K}^{-1}\mathbf{h} + \frac{1}{2}\log |\mathbf{K}| + \frac{N}{2}\log(2\pi), \quad (6)$$

where  $\mathbf{h} = \begin{bmatrix} \mathbf{h}^n \\ \mathbf{h}^{n-1} \end{bmatrix}$ ,  $p(\mathbf{h}|\theta, \lambda, \sigma^2) = \mathcal{N}(\mathbf{0}, \mathbf{K})$ , and  $\mathbf{K}$  is given by

$$\mathbf{K} = \begin{bmatrix} k^{n,n}(\mathbf{x}^n, \mathbf{x}^n) & k^{n,n-1}(\mathbf{x}^n, \mathbf{x}^{n-1}) \\ k^{n-1,n}(\mathbf{x}^{n-1}, \mathbf{x}^n) & k^{n-1,n-1}(\mathbf{x}^{n-1}, \mathbf{x}^{n-1}) \end{bmatrix} + \sigma^2 \mathbf{I}.$$

Here,  $N$  is the total number of data points in  $\mathbf{h}$ . Moreover,  $\sigma^2$  is included to capture the noise in the data and is also learned by minimizing the negative log marginal likelihood. The implicit underlying assumption is that  $\mathbf{h}^n = h^n(\mathbf{x}^n) + \boldsymbol{\epsilon}^n$  and  $\mathbf{h}^{n-1} = h^{n-1}(\mathbf{x}^{n-1}) + \boldsymbol{\epsilon}^{n-1}$  with  $\boldsymbol{\epsilon}^n \sim \mathcal{N}(0, \sigma^2 \mathbf{I})$  and  $\boldsymbol{\epsilon}^{n-1} \sim \mathcal{N}(0, \sigma^2 \mathbf{I})$  being independent. It is worth mentioning that the marginal likelihood does not simply favor the models that fit the training data best. In fact, it induces an automatic trade-off between data-fit and model complexity. This effect is called Occam’s razor [20] after William of Occam (1285–1349), who encouraged simplicity in explanations by the principle: “plurality should not be assumed without necessity”. Specifically,

minimizing the term  $\mathbf{h}^T \mathbf{K}^{-1} \mathbf{h}$  in equation (6) targets fitting the training data, while the log-determinant term  $\log |\mathbf{K}|$  penalizes model complexity. This mechanism automatically meets the Occam’s razor principle, albeit at the computational cost of obtaining the Cholesky factorization of  $\mathbf{K}$  that are used to compute both the inverse and the determinant. This natural regularization mechanism is a key property of Gaussian process regression and it enables inferring the unknown model parameters from very few data while effectively guarding against overfitting. Regularization is an important factor even in cases where data is abundant as seen in the recently growing literature on discovering ordinary and partial differential equations from data using sparse regression techniques [21, 2]. Model training practically consists of minimizing equation (6) with respect to the model parameters and hyper-parameters, namely  $\{\theta, \lambda, \sigma^2\}$ . This defines a non-convex optimization problem, and the common practice of employing classical gradient descent algorithms may lead to a local minimum. Therefore, the proposed method is also susceptible to converging to a set of hyper-parameters that corresponds to a local minimum of the negative marginal log likelihood. This behavior is standard for many machine learning algorithms (e.g., Gaussian processes, neural networks) [5], and the efficient *global* optimization still remains an open problem. In practice, this issue is addressed by solving the optimization problem from different hyper-parameter initializations, and returning the solution that yields the smallest negative marginal log likelihood. Although this still does not guarantee convergence to a global optimum, it is usually sufficient for obtaining a good solution. Moreover, the most computationally intensive part of training is associated with inverting dense covariance matrices  $\mathbf{K}$ . This scales cubically with the number  $N$  of training data in  $\mathbf{h}$ . Although this scaling is a well-known limitation of Gaussian process regression, it must be emphasized that it has been effectively addressed by the recent works of [22, 23, 24]. Furthermore, it should be highlighted that, although not pursued here, a fully Bayesian [25] and more robust estimate of the linear operator parameters  $\lambda$  can be obtained by assigning priors on  $\{\theta, \lambda, \sigma^2\}$ . However, this would require more costly sampling procedures such as Markov Chain Monte Carlo integration (see [5], chapter 5) to train the model.

## 5. Results

The proposed framework provides a general treatment of time-dependent and nonlinear partial differential equations, which can be of fundamentally different nature. This generality will be demonstrated by applying the algorithm to a dataset originally proposed in [2]. This dataset covers a wide range of canonical problems spanning a number of scientific domains including the Navier-Stokes, Schrödinger, and Kuramoto-Sivashinsky equations. Moreover, all data and codes used in this manuscript are publicly available on GitHub at <https://github.com/maziarraissi/HPM>.

### 5.1. Burgers' Equation

Burgers' equation is a fundamental partial differential equation arising in various areas of applied mathematics, including fluid mechanics, nonlinear acoustics, gas dynamics, and traffic flow [26]. It is derived from the Navier-Stokes equations for the velocity field by dropping the pressure gradient term. Burgers' equation, despite its relation to the much more complicated Navier-Stokes equations, does not exhibit turbulent behavior. However, for small values of the viscosity parameters, the Burger's equation leads to shock formation that is notoriously hard to resolve by classical numerical methods. In one space dimension the equation reads as

$$u_t + \lambda_1 uu_x - \lambda_2 u_{xx} = 0, \quad (7)$$

with  $(\lambda_1, \lambda_2)$  being the unknown parameters. The original data-set proposed in [2] contains 101 time snapshots of a solution to the Burgers' equation with a Gaussian initial condition, propagating into a traveling wave. The snapshots are  $\Delta t = 0.1$  apart. The spatial discretization of each snapshot involves a uniform grid with 256 elements. As depicted in figure 1 using only two of these snapshots (randomly selected) with 71 and 69 data points, respectively, the algorithm is capable of identifying the correct parameter values up to a relatively good accuracy. It should be highlighted that we are using only  $140 = 71 + 69$  data points out of a total of  $25856 = 101 \times 256$  in the original data set. This remarkable performance is achieved at the cost of explicitly encoding the underlying physical laws expressed by the Burgers' equation in the covariance functions of the *hidden physics model* (5). For a systematic study of the performance of the method, let us carry out the same experiment as the one illustrated in figure 1 for every two consecutive snapshots in the

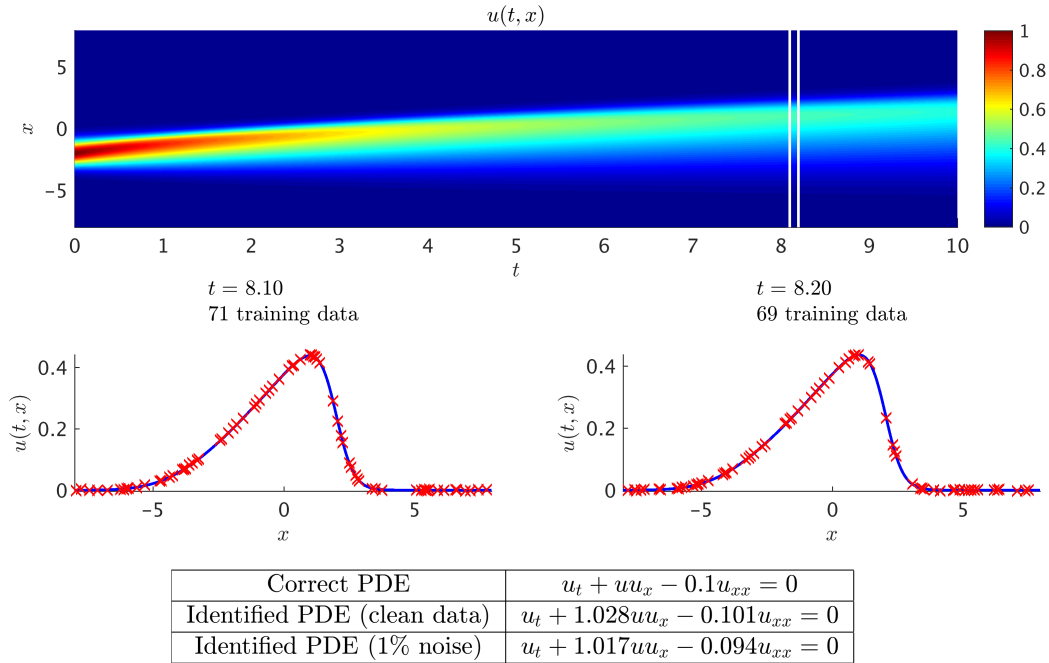


Figure 1: *Burgers' equation*: A solution to the Burgers' equation is depicted in the top panel. The two white vertical lines in this panel specify the locations of the two randomly selected snapshots. These two snapshots are  $\Delta t = 0.1$  apart and are plotted in the middle panel. The red crosses denote the locations of the training data points. The correct partial differential equation along with the identified ones are reported in the lower panel.

original dataset. We are still using the same number of data points (i.e., 71 and 69) for each pair of snapshots. The resulting statistics for the learned parameter values are reported in table 1. As is clearly demonstrated in this table, more noise in the data leads to less confidence in the estimated values for the parameters. Moreover, let us recall the main assumption of this work that the gap  $\Delta t$  between the pair of snapshots should be small enough so that we can employ the backward Euler scheme (see equation (2)). To test the importance of this assumption, let us use the exact same setup as the one explained in figure 1, but increase  $\Delta t$ . The results are reported in table 2. Therefore, the most important facts about the proposed methodology are that more data, less noise, and a smaller gap  $\Delta t$  between the two snapshots help the performance of the algorithm.

	Clean Data		1% Noise		5% Noise	
	$\lambda_1$	$\lambda_2$	$\lambda_1$	$\lambda_2$	$\lambda_1$	$\lambda_2$
First Quartile	1.0247	0.0942	0.9168	0.0784	0.3135	0.0027
Median	1.0379	0.0976	1.0274	0.0919	0.8294	0.0981
Third Quartile	1.0555	0.0987	1.1161	0.1166	1.2488	0.1543

Table 1: *Burgers' equation*: Resulting statistics for the learned parameter values.

		$\Delta t = 0.1$	$\Delta t = 0.5$	$\Delta t = 1.0$	$\Delta t = 1.5$
Clean Data	$\lambda_1$	1.0283	1.1438	1.2500	1.2960
	$\lambda_2$	0.1009	0.0934	0.0694	0.0431
1% Noise	$\lambda_1$	1.0170	1.1470	1.2584	1.3063
	$\lambda_2$	0.0935	0.0939	0.0711	0.0428

Table 2: *Burgers' equation*: Effect of increasing the gap  $\Delta t$  between the pair of snapshots.

## 5.2. The KdV Equation

The Korteweg-de Vries (KdV) equation is a mathematical model of waves on shallow water surfaces. It can also be viewed as Burgers' equation with an added dispersive term. The KdV equation has several connections to physical problems. It approximately describes the evolution of long, one-dimensional waves in many physical settings, including: shallow-water waves with weakly non-linear restoring forces, long internal waves in a density-stratified ocean, ion acoustic waves in a plasma, and acoustic waves on a crystal lattice. Moreover, the KdV equation is the governing equation of the string in the Fermi-Pasta-Ulam problem [27] in the continuum limit. The KdV equation reads as

$$u_t + \lambda_1 uu_x + \lambda_2 u_{xxx} = 0, \tag{8}$$

with  $(\lambda_1, \lambda_2)$  being the unknown parameters. The original dataset proposed in [2] contains a two soliton solution to the KdV equation with 512 spatial points and 201 time-steps. The snapshots are  $\Delta t = 0.1$  apart. As depicted in figure 2 using only two of these snapshots (randomly selected) with 111 and 109 data points, respectively, the algorithm is capable of identifying the correct parameter values up to a relatively good accuracy. In particular, we are using  $220 = 111 + 109$  out of a total of  $102912 = 201 \times 512$  data points in the original data set. This level of efficiency is a direct consequence of equation (5) where the covariance functions explicitly encode the underlying

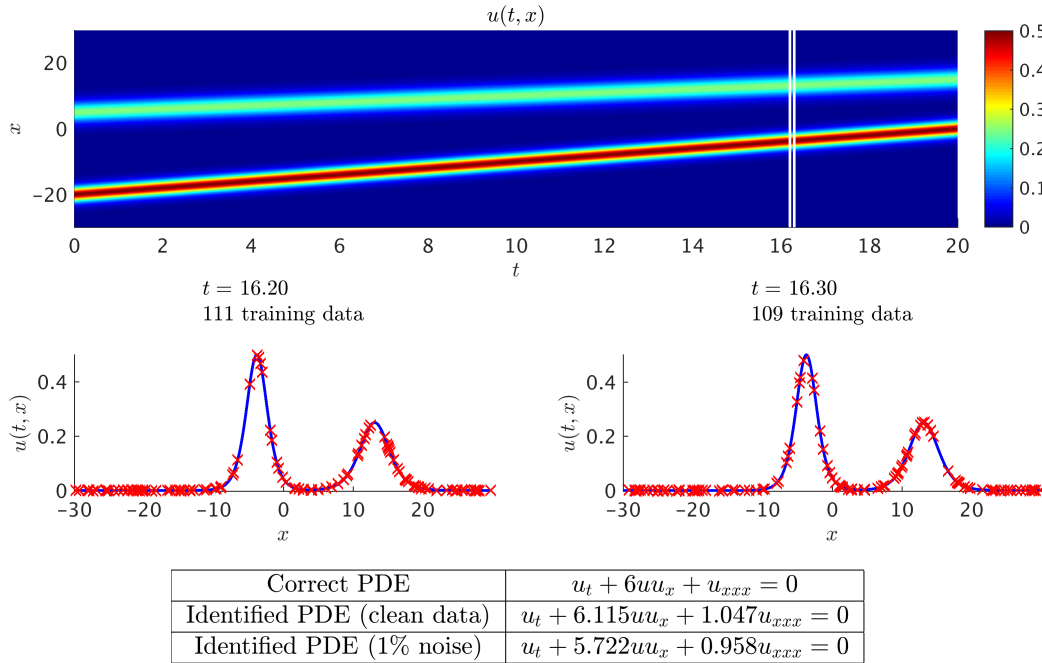


Figure 2: *The KdV equation*: A solution to the KdV equation is depicted in the top panel. The two white vertical lines in this panel specify the locations of the two randomly selected snapshots. These two snapshots are  $\Delta t = 0.1$  apart and are plotted in the middle panel. The red crosses denote the locations of the training data points. The correct partial differential equation along with the identified ones are reported in the lower panel.

physical laws expressed by the KdV equation.

### 5.3. Kuramoto-Sivashinsky Equation

The Kuramoto-Sivashinsky equation has similarities with Burgers' equation. However, because of the presence of both second and fourth order spatial derivatives, its behavior is far more complicated and interesting. The Kuramoto-Sivashinsky is a canonical model of a pattern forming system with spatio-temporal chaotic behavior. The sign of the second derivative term is such that it acts as an energy source and thus has a destabilising effect. The nonlinear term, however, transfers energy from low to high wave numbers where the stabilising fourth derivative term dominates. The first derivation of this equation was by Kuramoto in the study of reaction-diffusion equations modeling the Belousov-Zabotinskii reaction. The equation was also developed by Sivashinsky in higher space dimensions in modeling small ther-

mal diffusive instabilities in laminar flame fronts and in small perturbations from a reference Poiseuille flow of a film layer on an inclined plane. In one space dimension it has also been used as a model for the problem of Bénard convection in an elongated box, and it may be used to describe long waves on the interface between two viscous fluids and unstable drift waves in plasmas. In one space dimension the Kuramoto-Sivashinsky equation reads as

$$u_t + \lambda_1 uu_x + \lambda_2 u_{xx} + \lambda_3 u_{xxx} = 0, \quad (9)$$

where  $(\lambda_1, \lambda_2, \lambda_3)$  are the unknown parameters. The original dataset proposed in [2] contains a direct numerical solution of the Kuramoto-Sivashinsky equation with 1024 spatial points and 251 time-steps. The snapshots are  $\Delta t = 0.4$  apart. As depicted in figure 3 using only two of these snapshots (randomly selected) with 301 and 299 data points, respectively, the algorithm is capable of identifying the correct parameter values up to a relatively good accuracy. In particular, we are using  $600 = 301 + 299$  out of a total of  $257024 = 251 \times 1024$  data points in the original data set. This is possible because of equation (5) where the covariance functions explicitly encode the underlying physical laws expressed by the Kuramoto-Sivashinsky equation.

#### 5.4. Nonlinear Schrödinger Equation

The one-dimensional nonlinear Schrödinger equation is a classical field equation that is used to study nonlinear wave propagation in optical fibers and/or waveguides, Bose-Einstein condensates, and plasma waves. In optics, the nonlinear term arises from the intensity dependent index of refraction of a given material. Similarly, the nonlinear term for Bose-Einstein condensates is a result of the mean-field interactions of an interacting, N-body system. The nonlinear Schrödinger equation is given by

$$ih_t + \lambda_1 h_{xx} + \lambda_2 |h|^2 h = 0, \quad (10)$$

where  $(\lambda_1, \lambda_2)$  are the unknown parameters. Let  $u$  denote the real part of  $h$  and  $v$  the imaginary part. Then, the nonlinear Schrödinger equation can be equivalently written as

$$\begin{aligned} u_t + \lambda_1 v_{xx} + \lambda_2 (u^2 + v^2)v &= 0, \\ v_t - \lambda_1 u_{xx} - \lambda_2 (u^2 + v^2)u &= 0. \end{aligned} \quad (11)$$

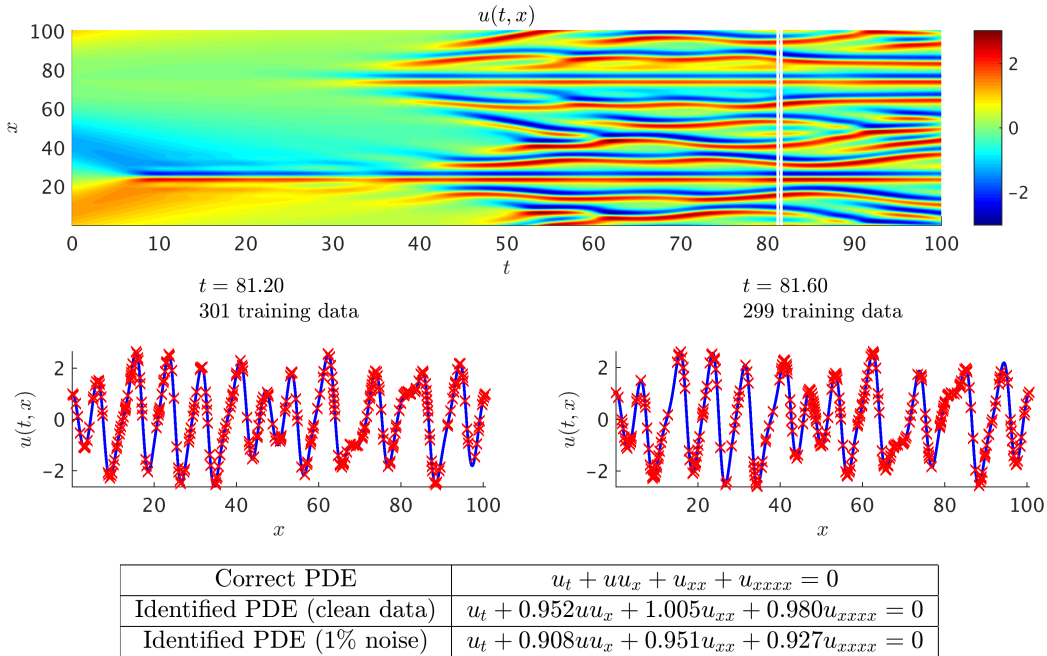


Figure 3: *Kuramoto-Sivashinsky Equation*: A solution to the Kuramoto-Sivashinsky equation is depicted in the top panel. The two white vertical lines in this panel specify the locations of the two randomly selected snapshots. These two snapshots are  $\Delta t = 0.4$  apart and are plotted in the middle panel. The red crosses denote the locations of the training data points. The correct partial differential equation along with the identified ones are reported in the lower panel.

Employing the backward Euler time stepping scheme, we obtain

$$\begin{aligned} u^n + \Delta t \lambda_1 v_{xx}^n + \Delta t \lambda_2 [(u^n)^2 + (v^n)^2] v^n &= u^{n-1}, \\ v^n - \Delta t \lambda_1 u_{xx}^n - \Delta t \lambda_2 [(u^n)^2 + (v^n)^2] u^n &= v^{n-1}. \end{aligned} \quad (12)$$

The above equations can be approximated by

$$\begin{aligned} u^n + \Delta t \lambda_1 v_{xx}^n + \Delta t \lambda_2 [(u^{n-1})^2 + (v^{n-1})^2] v^n &= u^{n-1}, \\ v^n - \Delta t \lambda_1 u_{xx}^n - \Delta t \lambda_2 [(u^{n-1})^2 + (v^{n-1})^2] u^n &= v^{n-1}, \end{aligned} \quad (13)$$

which involves only linear operations. Here,  $u^{n-1}(x)$  and  $v^{n-1}(x)$  are the real and imaginary parts of the state of the system at the previous time step. We proceed by placing two independent Gaussian processes on  $u^n(x)$  and  $v^n(x)$ ;

i.e.,

$$\begin{aligned} u^n(x) &\sim \mathcal{GP}(0, k_u(x, x'; \theta_u)), \\ v^n(x) &\sim \mathcal{GP}(0, k_v(x, x'; \theta_v)). \end{aligned} \quad (14)$$

Here,  $\theta_u$  and  $\theta_v$  are the hyper-parameters of the kernels  $k_u$  and  $k_v$ , respectively. The prior assumptions (14) along with equations (13) enables us to encode the underlying laws of physics expressed by the nonlinear Schrödinger equation in the resulting *hidden physics model*

$$\begin{bmatrix} u^n \\ v^n \\ u^{n-1} \\ v^{n-1} \end{bmatrix} \sim \mathcal{GP} \left( 0, \begin{bmatrix} k_{u,u}^{n,n} & k_{u,v}^{n,n} & k_{u,u}^{n,n-1} & k_{u,v}^{n,n-1} \\ k_{v,u}^{n,n} & k_{v,v}^{n,n} & k_{v,u}^{n,n-1} & k_{v,v}^{n,n-1} \\ k_{u,u}^{n-1,n} & k_{u,v}^{n-1,n} & k_{u,u}^{n-1,n-1} & k_{u,v}^{n-1,n-1} \\ k_{v,u}^{n-1,n} & k_{v,v}^{n-1,n} & k_{v,u}^{n-1,n-1} & k_{v,v}^{n-1,n-1} \end{bmatrix} \right). \quad (15)$$

The specific forms of the covariance functions involved in model (15) is a direct function of the prior assumptions (14) as well as equations (13). The hyper-parameters  $\theta_u$  and  $\theta_v$  along with the parameters  $\lambda_1$  and  $\lambda_2$  are learned by minimizing the negative log marginal likelihood as outlined in section 4. The original data-set proposed in [2] contains 501 time snapshots of a solution to the nonlinear Schrödinger equation with a Gaussian initial condition. The snapshots are  $\Delta t = 0.0063$  apart. The spatial discretization of each snapshot involves a uniform grid with 512 elements. As depicted in figure 4 using only two of these snapshots (randomly selected) with 49 and 51 data points, respectively, the algorithm is capable of identifying the correct parameter values up to a relatively good accuracy. It should be highlighted that we are using only  $100 = 49 + 51$  data points out of a total of  $256512 = 501 \times 512$  in the original data set. This remarkable performance is achieved at the cost of explicitly encoding the underlying physical laws expressed by the nonlinear Schrödinger equation in the covariance functions of the *hidden physics model* (15).

### 5.5. Navier-Stokes Equations

Navier-Stokes equations describe the physics of many phenomena of scientific and engineering interest. They may be used to model the weather, ocean currents, water flow in a pipe and air flow around a wing. The Navier-Stokes equations in their full and simplified forms help with the design of aircraft and cars, the study of blood flow, the design of power stations, the analysis

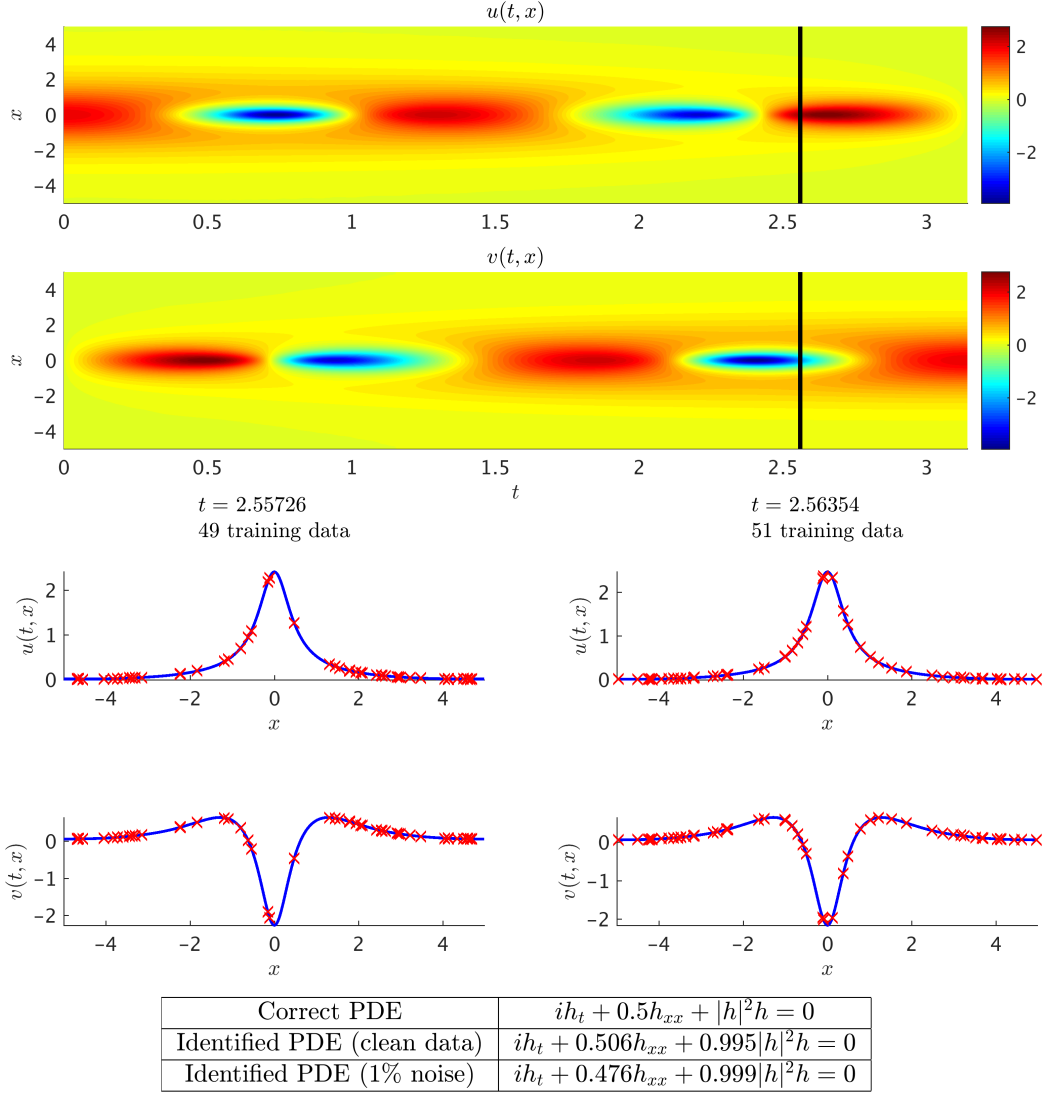


Figure 4: *Nonlinear Schrödinger Equation*: A solution to the nonlinear Schrödinger equation is depicted in the top two panels. The two black vertical lines in these two panels specify the locations of the two randomly selected snapshots. These two snapshots are  $\Delta t = 0.0063$  apart and are plotted in the two middle panels. The red crosses denote the locations of the training data points. The correct partial differential equation along with the identified ones are reported in the lower panel. Here,  $u$  is the real part of  $h$  and  $v$  is the imaginary part.

of pollution, and many other applications. Let us consider the Navier-Stokes equations in 2D given explicitly by

$$\begin{aligned} u_t + \lambda_1(uu_x + vv_y) &= -p_x + \lambda_2(u_{xx} + u_{yy}), \\ v_t + \lambda_1(uv_x + vv_y) &= -p_y + \lambda_2(v_{xx} + v_{yy}), \end{aligned} \quad (16)$$

where  $u(t, x, y)$  denotes the  $x$ -component of the velocity field,  $v(t, x, y)$  the  $y$ -component, and  $p(t, x, y)$  the pressure. Here,  $\lambda = (\lambda_1, \lambda_2)$  are the unknown parameters. Solutions to the Navier-Stokes equations are searched in the set of divergence-free functions; i.e.,

$$u_x + v_y = 0. \quad (17)$$

This extra equation is the continuity equation for incompressible fluids that describes the conservation of mass of the fluid. Applying the backward Euler time stepping scheme to the Navier-Stokes equations (16) we obtain

$$\begin{aligned} u^n + \Delta t \lambda_1(u^n u_x^n + v^n v_y^n) + \Delta t p_x^n - \Delta t \lambda_2(u_{xx}^n + u_{yy}^n) &= u^{n-1}, \\ v^n + \Delta t \lambda_1(u^n v_x^n + v^n v_y^n) + \Delta t p_y^n - \Delta t \lambda_2(v_{xx}^n + v_{yy}^n) &= v^{n-1}, \end{aligned} \quad (18)$$

where  $u^n(x, y) = u(t^n, x, y)$  and  $v^n(x, y) = v(t^n, x, y)$ . We make the assumption that

$$u^n = \psi_y^n, \quad v^n = -\psi_x^n, \quad (19)$$

for some latent function  $\psi^n(x, y)$ . Under this assumption, the continuity equation (17) will be automatically satisfied. We proceed by placing a Gaussian process prior on

$$\psi^n(x, y) \sim \mathcal{GP}(0, k((x, y), (x', y'); \theta)), \quad (20)$$

where  $\theta$  are the hyper-parameters of the kernel  $k((x, y), (x', y'); \theta)$ . This will result in the following multi-output Gaussian process

$$\begin{bmatrix} u^n \\ v^n \end{bmatrix} \sim \mathcal{GP}\left(0, \begin{bmatrix} k_{u,u}^{n,n} & k_{u,v}^{n,n} \\ k_{v,u}^{n,n} & k_{v,v}^{n,n} \end{bmatrix}\right), \quad (21)$$

where

$$\begin{aligned} k_{u,u}^{n,n} &= \frac{\partial}{\partial y} \frac{\partial}{\partial y'} k, & k_{u,v}^{n,n} &= -\frac{\partial}{\partial y} \frac{\partial}{\partial x'} k, \\ k_{v,u}^{n,n} &= -\frac{\partial}{\partial x} \frac{\partial}{\partial y'} k, & k_{v,v}^{n,n} &= \frac{\partial}{\partial x} \frac{\partial}{\partial x'} k. \end{aligned}$$

By construction, any samples generated from this multi-output Gaussian process will satisfy the continuity equation. Moreover, independent from  $\psi^n(x, y)$ , we will place a Gaussian process prior on  $p^n(x, y)$ ; i.e.,

$$p^n(x, y) \sim \mathcal{GP}(0, k_{p,p}^{n,n}((x, y), (x', y'); \theta_p)). \quad (22)$$

We linearize the Euler time stepping scheme by employing the states  $u^{n-1}(x, y)$  and  $v^{n-1}(x, y)$  of the system at the previous time step and writing

$$\begin{aligned} u^n + \Delta t \lambda_1 (u^{n-1} u_x^n + v^{n-1} u_y^n) + \Delta t p_x^n - \Delta t \lambda_2 (u_{xx}^n + u_{yy}^n) &= u^{n-1}, \\ v^n + \Delta t \lambda_2 (u^{n-1} v_x^n + v^{n-1} v_y^n) + \Delta t p_y^n - \Delta t \lambda_2 (v_{xx}^n + v_{yy}^n) &= v^{n-1}. \end{aligned} \quad (23)$$

The above equations (23) can be rewritten as

$$\begin{aligned} \mathcal{L}_{(x,y)}^\lambda u^n + \Delta t p_x^n &= u^{n-1}, \\ \mathcal{L}_{(x,y)}^\lambda v^n + \Delta t p_y^n &= v^{n-1}. \end{aligned} \quad (24)$$

by defining the linear operator  $\mathcal{L}_{(x,y)}^\lambda$  to be given by

$$\mathcal{L}_{(x,y)}^\lambda h := h + \Delta t \lambda_1 (u^{n-1} h_x + v^{n-1} h_y) - \Delta t \lambda_2 (h_{xx} + h_{yy}). \quad (25)$$

This will allow us to obtain the following *hidden physics model* encoding the structure of the Navier-Stokes equations and the backward Euler time stepping scheme in its kernels; i.e.,

$$\begin{bmatrix} u^n \\ v^n \\ p^n \\ u^{n-1} \\ v^{n-1} \end{bmatrix} \sim \mathcal{GP} \left( 0, \begin{bmatrix} k_{u,u}^{n,n} & k_{u,v}^{n,n} & 0 & k_{u,u}^{n,n-1} & k_{u,v}^{n,n-1} \\ & k_{v,v}^{n,n} & 0 & k_{v,u}^{n,n-1} & k_{v,v}^{n,n-1} \\ & & k_{p,p}^{n,n} & k_{p,u}^{n,n-1} & k_{p,v}^{n,n-1} \\ & & & k_{u,u}^{n-1,n-1} & k_{u,v}^{n-1,n-1} \\ & & & & k_{v,v}^{n-1,n-1} \end{bmatrix} \right), \quad (26)$$

where

$$\begin{aligned}
k_{u,u}^{n,n-1} &= \mathcal{L}_{(x',y')}^\lambda k_{u,u}^{n,n}, & k_{u,v}^{n,n-1} &= \mathcal{L}_{(x',y')}^\lambda k_{u,v}^{n,n}, \\
k_{v,u}^{n,n-1} &= \mathcal{L}_{(x',y')}^\lambda k_{v,u}^{n,n}, & k_{v,v}^{n,n-1} &= \mathcal{L}_{(x',y')}^\lambda k_{v,v}^{n,n}, \\
k_{p,u}^{n,n-1} &= \Delta t \frac{\partial}{\partial x'} k_{p,p}^{n,n}, & k_{p,v}^{n,n-1} &= \Delta t \frac{\partial}{\partial y'} k_{p,p}^{n,n},
\end{aligned}$$

and

$$\begin{aligned}
k_{u,u}^{n-1,n-1} &= \mathcal{L}_{(x,y)}^\lambda k_{u,u}^{n,n-1} + \Delta t \frac{\partial}{\partial x} k_{p,u}^{n,n-1}, \\
k_{u,v}^{n-1,n-1} &= \mathcal{L}_{(x,y)}^\lambda k_{u,v}^{n,n-1} + \Delta t \frac{\partial}{\partial x} k_{p,v}^{n,n-1}, \\
k_{v,v}^{n-1,n-1} &= \mathcal{L}_{(x,y)}^\lambda k_{v,v}^{n,n-1} + \Delta t \frac{\partial}{\partial y} k_{p,v}^{n,n-1}.
\end{aligned}$$

The lower triangular portion of the matrix of covariance functions (26) is not shown due to symmetry. The hyper-parameters  $\theta$  and  $\theta_p$  along with the parameters  $\lambda_1$  and  $\lambda_2$  are learned by minimizing the negative log marginal likelihood as outlined in section 4. Following the exact same instructions as the ones provided in [28] and [2], we simulate the Navier-Stokes equations describing the two-dimensional fluid flow past a circular cylinder at Reynolds number 100 using the Immersed Boundary Projection Method [29, 30]. This approach utilizes a multi-domain scheme with four nested domains, each successive grid being twice as large as the previous. Length and time are nondimensionalized so that the cylinder has unit diameter and the flow has unit velocity. Data is collected on the finest domain with dimensions  $9 \times 4$  at a grid resolution of  $449 \times 199$ . The flow solver uses a 3rd-order Runge Kutta integration scheme with a time step of  $t = 0.02$ , which has been verified to yield well-resolved and converged flow fields. After simulations converge to steady-state vortex shedding, flow snapshots are saved every  $\Delta t = 0.02$ . As depicted in figure 5 using only two snapshots of the velocity field with 251 and 249 data points, respectively, the algorithm is capable of identifying the correct parameter values up to a relatively good accuracy. It should be highlighted that we are using only two snapshots with a total of  $500 = 251 + 249$  data points. This remarkable performance is achieved at the cost of explicitly encoding the underlying physical laws expressed by the Navier-Stokes equations in the covariance functions of the *hidden physics*

model (26).

### 5.6. Fractional Equations

Let us consider the one dimensional fractional equation

$$u_t - \lambda_1 \mathcal{D}_{-\infty, x}^{\lambda_2} u = 0, \quad (27)$$

where  $(\lambda_1, \lambda_2)$  are the unknown parameters. In particular,  $\lambda_2$  is the fractional order of the operator  $\mathcal{D}_{-\infty, x}^{\lambda_2}$  that is defined in the Riemann-Liouville sense [31]. Fractional operators often arise in modeling anomalous diffusion processes and other non-local interactions. Integer values such as  $\lambda_2 = 1$  and  $\lambda_2 = 2$  can model classical advection and diffusion phenomena, respectively. However, under the fractional calculus setting,  $\lambda_2$  can assume real values and thus continuously interpolate between inherently different model behaviors. The proposed framework allows  $\lambda_2$  to be directly inferred from noisy data, and opens the path to a flexible formalism for model discovery and calibration. Applying the backward Euler time stepping scheme to equation (27) we obtain

$$u^n - \Delta t \lambda_1 \mathcal{D}_{-\infty, x}^{\lambda_2} u^n = u^{n-1}. \quad (28)$$

Here,  $u^n(x) = u(t^n, x)$  is the hidden state of the system at time  $t^n$ . We make the prior assumption that

$$u^n(x) \sim \mathcal{GP}(0, k(x, x'; \theta)). \quad (29)$$

The prior assumption (29) along with the backward Euler scheme (28) allow us to obtain the following *hidden physics model* corresponding to the fractional equation (27); i.e.,

$$\begin{bmatrix} u^n \\ u^{n-1} \end{bmatrix} \sim \mathcal{GP} \left( 0, \begin{bmatrix} k^{n,n} & k^{n,n-1} \\ k^{n-1,n} & k^{n-1,n-1} \end{bmatrix} \right). \quad (30)$$

The only technicality induced by fractional operators has to do with deriving the kernels  $k^{n,n-1}$ ,  $k^{n-1,n}$ , and  $k^{n-1,n-1}$ . Here,  $k^{n,n-1}(x, x'; \theta, \lambda_1, \lambda_2)$  was obtained by taking the inverse Fourier transform [31] of

$$[1 - \Delta t \lambda_1 (-iw')^{\lambda_2}] \widehat{k}(w, w'; \theta),$$

where  $\widehat{k}(w, w'; \theta)$  is the Fourier transform of the kernel  $k(x, x'; \theta)$ . Similarly, one can obtain  $k^{n-1,n}$  and  $k^{n-1,n-1}$ . The hyper-parameters  $\theta$  along with the

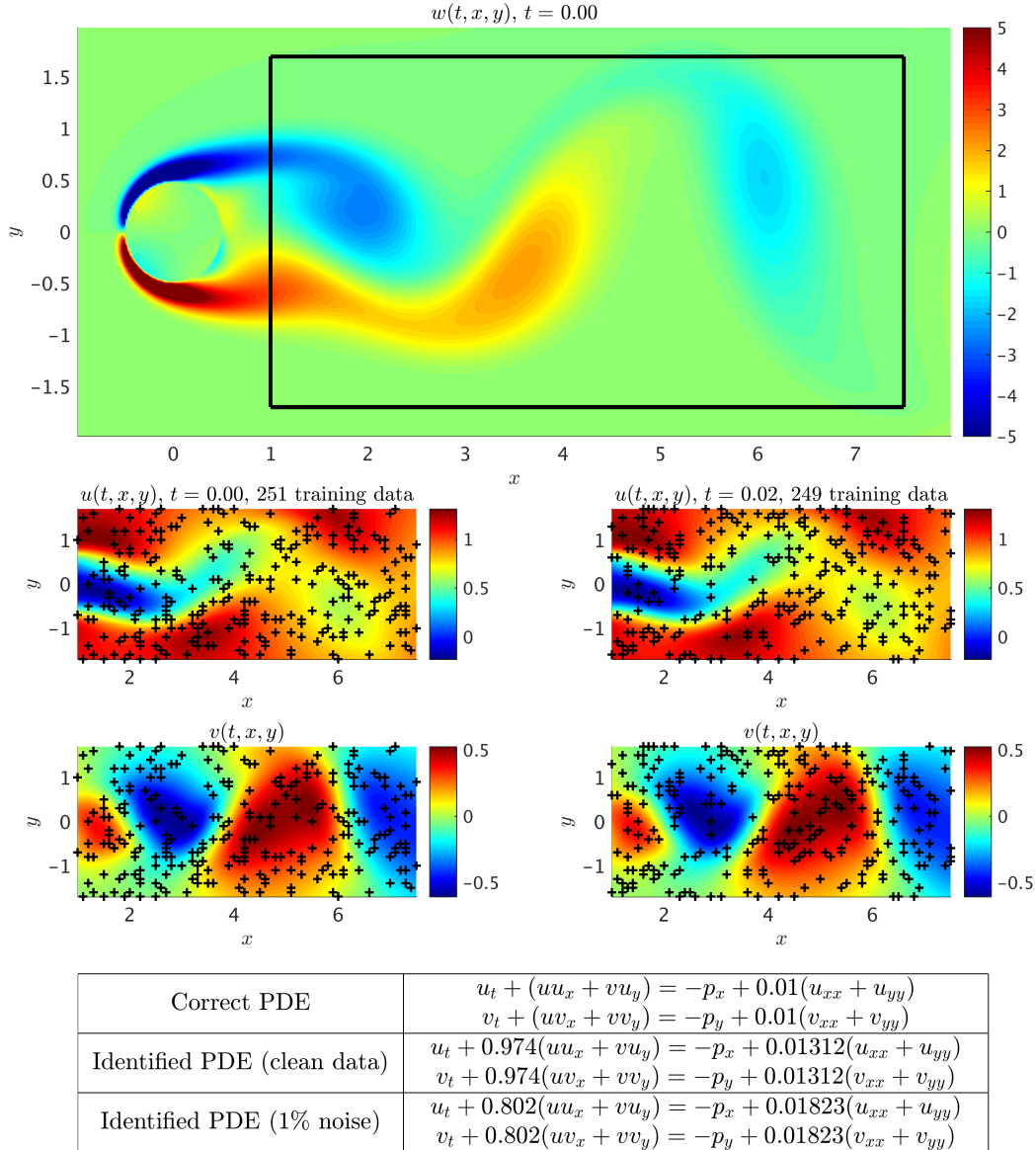


Figure 5: *Navier-Stokes Equations*: A single snapshot of the vorticity field of a solution to the Navier-Stokes equations for the fluid flow past a cylinder is depicted in the top panel. The black box in this panel specifies the sampling region. Two snapshots of the velocity field being  $\Delta t = 0.02$  apart are plotted in the two middle panels. The black crosses denote the locations of the training data points. The correct partial differential equation along with the identified ones are reported in the lower panel. Here,  $u$  denotes the  $x$ -component of the velocity field,  $v$  the  $y$ -component, and  $w$  the vorticity field.

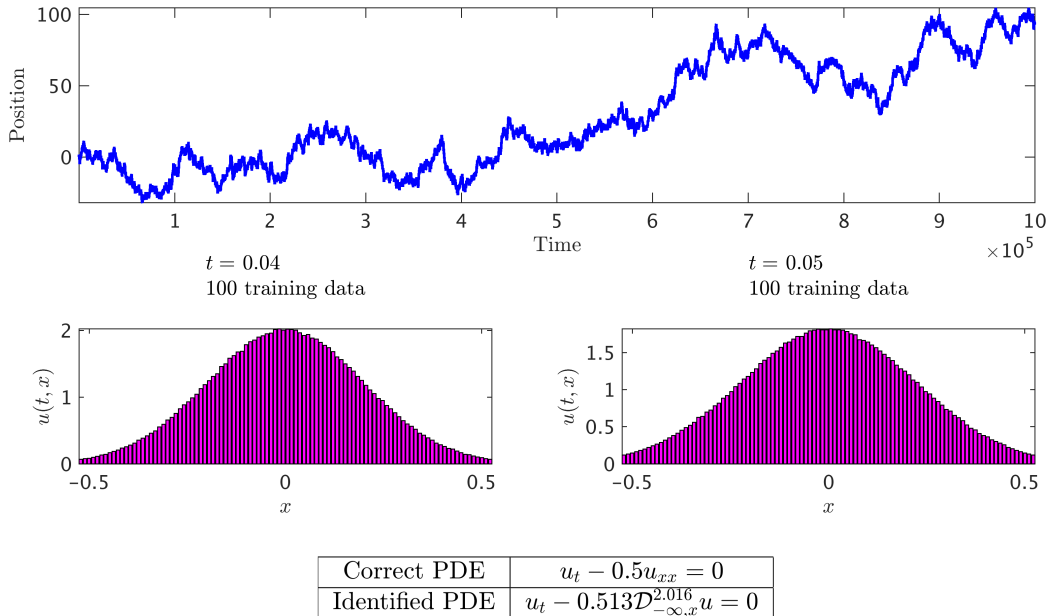


Figure 6: *Fractional Equation*: A single realization of a Brownian motion is depicted in the top panel. Two histograms of the particle’s displacement, being  $\Delta t = 0.01$  apart, are plotted in the middle panel. The correct partial differential equation along with the identified ones are reported in the lower panel.

parameters  $\lambda_1$  and  $\lambda_2$  are learned by minimizing the negative log marginal likelihood as outlined in section 4. We use the hidden physics model (30) to identify the long celebrated relation between Brownian motion and the diffusion equation [2]. The Fokker-Planck equation for a Brownian motion with  $x(t + \Delta t) \sim \mathcal{N}(x(t), dt)$ , associated with a particle’s position, is  $u_t = 0.5u_{xx}$ . We simulated a Brownian motion at evenly spaced time points and generated two histograms of the particle’s displacement. These two histograms are  $\Delta t = 0.01$  apart. As depicted in figure 6 using only two histograms with 100 bins for each one, the algorithm is capable of identifying the correct fractional order and parameter values up to a relatively good accuracy.

## 6. Discussion

In summary, this work introduced a structured learning machine which is explicitly informed by the underlying physics that possibly generated the observed data. Exploiting this structure is critical for constructing data-efficient learning algorithms that can effectively distill information in the

data-scarce scenarios appearing routinely when we study complex physical systems. We applied the proposed framework to the problem of identifying general parametric nonlinear partial differential equations from noisy data. This generality was demonstrated using various benchmark problems with different attributes. This work should be considered a direct follow up on [1] in which a similar technology was employed to infer solutions to time-dependent and nonlinear partial differential equations, and effectively quantify and propagate uncertainty due to noisy initial or boundary data. The ideas introduced in these two papers provide a natural platform for learning from noisy data and computing under uncertainty. Perhaps the most pressing limitation of this work in its present form stems from the cubic scaling with respect to the total number of training data points. However, ideas such as recursive Kalman updates [32], variational inference [23], and parametric Gaussian processes [24] can be used to address this limitation. In terms of future work, we plan to leverage the proposed framework to study problems in control theory using state-space representations.

## Acknowledgements

This work received support by the DARPA EQUiPS grant N66001-15-2-4055, the MURI/ARO grant W911NF-15-1-0562, and the AFOSR grant FA9550-17-1-0013. All data and codes used in this manuscript are publicly available on GitHub at <https://github.com/maziarraissi/HPM>.

## References

- [1] M. Raissi, P. Perdikaris, G. E. Karniadakis, Numerical gaussian processes for time-dependent and non-linear partial differential equations, arXiv preprint arXiv:1703.10230 (2017).
- [2] S. H. Rudy, S. L. Brunton, J. L. Proctor, J. N. Kutz, Data-driven discovery of partial differential equations, *Science Advances* 3 (2017).
- [3] M. Raissi, P. Perdikaris, G. E. Karniadakis, Inferring solutions of differential equations using noisy multi-fidelity data, *Journal of Computational Physics* 335 (2017) 736 – 746.
- [4] M. Raissi, G. E. Karniadakis, Machine learning of linear differential equations using Gaussian processes, arXiv preprint arXiv:1701.02440 (2017).

- [5] C. E. Rasmussen, Gaussian processes for machine learning, MIT Press, 2006.
- [6] K. P. Murphy, Machine learning: a probabilistic perspective, MIT press, 2012.
- [7] V. Vapnik, The nature of statistical learning theory, Springer Science & Business Media, 2013.
- [8] B. Schölkopf, A. J. Smola, Learning with kernels: support vector machines, regularization, optimization, and beyond, MIT press, 2002.
- [9] M. E. Tipping, Sparse Bayesian learning and the relevance vector machine, *The journal of machine learning research* 1 (2001) 211–244.
- [10] A. Tikhonov, Solution of incorrectly formulated problems and the regularization method, in: *Soviet Math. Dokl.*, volume 5, pp. 1035–1038.
- [11] A. N. Tikhonov, V. Y. Arsenin, *Solutions of Ill-posed problems*, W.H. Winston, 1977.
- [12] T. Poggio, F. Girosi, Networks for approximation and learning, *Proceedings of the IEEE* 78 (1990) 1481–1497.
- [13] R. M. Neal, *Bayesian learning for neural networks*, volume 118, Springer Science & Business Media, 2012.
- [14] N. Aronszajn, Theory of reproducing kernels, *Transactions of the American Mathematical Society* 68 (1950) 337–404.
- [15] S. Saitoh, *Theory of reproducing kernels and its applications*, volume 189, Longman, 1988.
- [16] A. Berlinet, C. Thomas-Agnan, *Reproducing kernel Hilbert spaces in probability and statistics*, Springer Science & Business Media, 2011.
- [17] R. Calandra, J. Peters, C. E. Rasmussen, M. P. Deisenroth, Manifold gaussian processes for regression, in: *Neural Networks (IJCNN)*, 2016 International Joint Conference on, IEEE, pp. 3338–3345.
- [18] M. Raissi, G. Karniadakis, Deep multi-fidelity gaussian processes, arXiv preprint arXiv:1604.07484 (2016).

- [19] D. C. Liu, J. Nocedal, On the limited memory bfgs method for large scale optimization, *Mathematical programming* 45 (1989) 503–528.
- [20] C. E. Rasmussen, Z. Ghahramani, Occam’s razor, *Advances in neural information processing systems* (2001) 294–300.
- [21] S. L. Brunton, J. L. Proctor, J. N. Kutz, Discovering governing equations from data by sparse identification of nonlinear dynamical systems, *Proceedings of the National Academy of Sciences* 113 (2016) 3932–3937.
- [22] E. Snelson, Z. Ghahramani, Sparse gaussian processes using pseudo-inputs, in: *Advances in neural information processing systems*, pp. 1257–1264.
- [23] J. Hensman, N. Fusi, N. D. Lawrence, Gaussian processes for big data, *arXiv preprint arXiv:1309.6835* (2013).
- [24] M. Raissi, Parametric gaussian process regression for big data, *arXiv preprint arXiv:1704.03144* (2017).
- [25] A. M. Stuart, Inverse problems: a bayesian perspective, *Acta Numerica* 19 (2010) 451–559.
- [26] C. Basdevant, M. Deville, P. Haldenwang, J. Lacroix, J. Ouazzani, R. Peyret, P. Orlandi, A. Patera, Spectral and finite difference solutions of the Burgers equation, *Computers & fluids* 14 (1986) 23–41.
- [27] T. Dauxois, Fermi, pasta, ulam and a mysterious lady, *arXiv preprint arXiv:0801.1590* (2008).
- [28] J. N. Kutz, S. L. Brunton, B. W. Brunton, J. L. Proctor, *Dynamic Mode Decomposition: Data-Driven Modeling of Complex Systems*, SIAM, 2016.
- [29] K. Taira, T. Colonius, The immersed boundary method: a projection approach, *Journal of Computational Physics* 225 (2007) 2118–2137.
- [30] T. Colonius, K. Taira, A fast immersed boundary method using a nullspace approach and multi-domain far-field boundary conditions, *Computer Methods in Applied Mechanics and Engineering* 197 (2008) 2131–2146.

- [31] I. Podlubny, Fractional differential equations: an introduction to fractional derivatives, fractional differential equations, to methods of their solution and some of their applications, volume 198, Academic press, 1998.
- [32] J. Hartikainen, S. Särkkä, Kalman filtering and smoothing solutions to temporal Gaussian process regression models, in: Machine Learning for Signal Processing (MLSP), 2010 IEEE International Workshop on, IEEE, pp. 379–384.